JOURNAL OF AIRCRAFT
Vol. 31, No. 3, May–June 1994

Two-Dimensional Euler Zonal Method Using Composite Structured and Unstructured Meshes

H. Hefazi* and V. Chin†
California State University, Long Beach, Long Beach, California 90840
and
L. T. Chen‡
Douglas Aircraft Company, Long Beach, California 90846

A two-dimensional zonal interactive scheme, based on Euler equations, has been developed for computing flows about complex geometries. A composite structured and unstructured grid, using conformal mapping and Delaunay triangulation, respectively, is first generated about the geometry. The finite-volume Euler method is then modified to couple zones with structured and unstructured grids. Solutions about multielement airfoils and iced airfoils are given as examples of the applications of the scheme. The zonal interaction scheme and accuracy and efficiency of the solutions are discussed.

I. Introduction

IN recent years the increasing availability of large-scale computing resources, together with the practical interest in transonic aerodynamics, has led to major advances in the calculation of transonic flows over complex geometries. The development of new methods for mesh generation has been essential to this progress since accurate and efficient solutions of the governing equations around complex geometries require the generation of suitable meshes.

Although many methods have been developed for the generation of structured grid around simple geometries, few can be extended to complicated two- and three-dimensional shapes such as multielement airfoil or multicomponent aircraft configurations. Also, in many applications of structured grids, the quality of the generated mesh is not uniform throughout the computational domain. This can cause considerable problems in specific regions of importance. For this reason triangular (tetrahedral) meshes have proven very attractive, since relatively complex geometries can be meshed efficiently, and an almost arbitrary degree of mesh adaption and refinement can be achieved by the addition of control points. Furthermore, the development of flow algorithms which do not depend on the inherent structure of the grid points have eliminated the restriction of grid structure and made triangles and tetrahedrons suitable shapes with which to resolve complicated geometric regions.

A wide variety of algorithms have been devised for the generation of unstructured triangular meshes. Among the different approaches, the Delaunay triangulation algorithm[1] is most commonly used. An essential requirement for obtaining satisfactory meshes when using the Delaunay triangulator is the appropriate placement of interior points, since this scheme gives no guidance on where to place the mesh points. Inappropriate placement of mesh points results in poor quality meshes even though they may satisfy the Delaunay criteria. Therefore, certain criterion for introducing interior mesh points has to be established before applying the Delaunay triangulation.

The debate over relative advantages of structured and unstructured grid methods is an ongoing matter. While unstructured grid methods have the clear advantage in that they can treat complicated problems such as a complete aircraft configuration under static or dynamic deformation,[2] they have been regarded as less efficient and less accurate than their structured counterparts.[3,4] Although it is shown that careful attention to the quality of the grid and use of efficient gather-scatter routines can result in methods that have accuracy and efficiency equivalent to current structured solvers[4] (at least in two-dimensional problems), lack of robust acceleration techniques, such as multigrid schemes (for three-dimensional problems), is a clear disadvantage. Furthermore, even though other algorithms such as direct and implicit solvers and finite-volume methods have been developed for unstructured grids, in general these algorithms are not as efficient and effective as their structured counterparts.[5,6] Structured flow solvers have many other highly desirable features such as efficient grid generation techniques and smaller computer time and memory requirements.

An efficient way of analyzing a complex geometry of several components is through a zonal approach, using composite structured and unstructured grids. This approach requires considerably less memory than using an entire unstructured mesh capable of handling the same geometry. While for two-dimensional inviscid flows the increased efficiency and memory savings may not be an important issue, extension of this approach to viscous or three-dimensional problems will result in substantial overhead reduction.

A composite approach has several other potential advantages. For example, in problems requiring dynamic mesh due to continuous change of the geometry, a composite approach enables the regridding of only a small portion of the domain where the change occurs. Triangular meshes could also be used to link zones with different structured grid topologies such as C, H, and O grids, which may be needed due to different geometry requirements. In another application,[7] a composite approach has been used to solve the viscous flow near the surface boundaries, utilizing a structured O-mesh in this region, while using a triangular-based Euler method in the outer region. This approach addresses the accuracy problems associated with highly stretched triangular grids that would have been needed in the viscous region, as well as allowing the implementation of higher-order, implicit schemes for viscous flow calculations.

Presented as Paper 90-3050 at the AIAA 8th Applied Aerodynamics Conference, Portland, OR, Aug. 20–22, 1990; received May 8, 1992; revision received May 27, 1993; accepted for publication May 27, 1993.

*Associate Professor, Aerospace Engineering Department. Senior Member AIAA.

†Graduate Student, Aerospace Engineering Department. Member AIAA.

‡Senior Principal Engineer/Scientist. Senior Member AIAA.

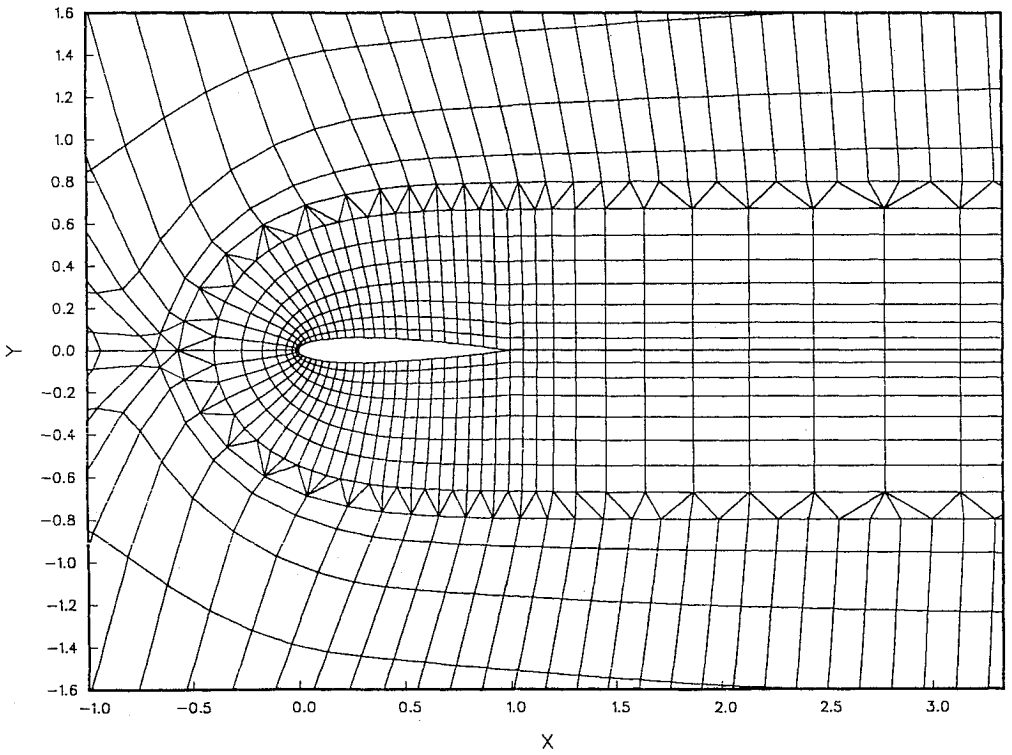

Fig. 1 Triangular meshes, used in boundary region to serve as a link between discontinuous H and C meshes.

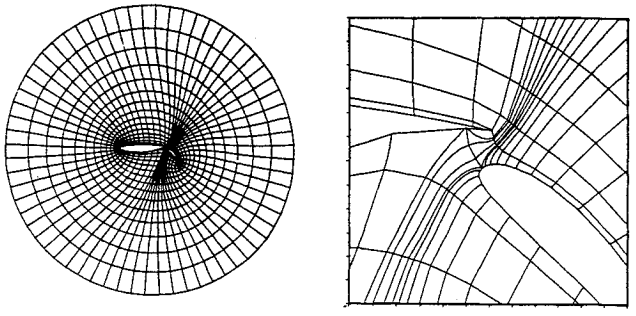

Fig. 2 Structured grid for a two-element airfoil with large flap deflection.

In this article, in view of these desirable, potential applications of a composite approach, a general two-dimensional zonal boundary interaction scheme which utilizes combinations of structured and unstructured mesh types is presented. Solutions for flow about multielement and iced airfoils are given as examples of some of the above-mentioned applications of the scheme.

II. Grid Generation

The grid-generation process begins with the generation of a base grid which encompasses the entire flowfield. Regions of undesirable grid quality are then identified and categorized as subsequent unstructured-mesh zones. Triangular grids are produced in these regions using existing mesh points and additional points as necessary. In an alternate approach, the domains for structured and unstructured grids are first identified, in such a way that the geometry combined with the unstructured grid zone forms a simpler geometry. Structured grids can then be generated for this modified geometry. Using the boundary points and additional points as needed, the "masked out" region will then be triangulated. Local triangulation can also be used, e.g., at boundaries where grid lines have discontinuities due to the requirements of the grid generation methods of different zones.

In Fig. 1, the C- and H-mesh lines of a hybrid mesh around a NACA 0012 airfoil generated by conformal mapping, are shown to be discontinuous, allowing a more independent grid generation in each zone. This feature could be very useful in more complicated geometries where different components may have different grid-generation requirements. One or several layers of triangular meshes can be used as a link between structured C and H meshes. This example uses existing boundary points to generate a layer of triangular elements for this purpose.

A more complex example is the multielement airfoil of Fig. 2. A grid-generation method for this airfoil has been developed by Halsey[8] using a conformal mapping technique. The main airfoil and flap are first linked together, forcing a continuous surface. This surface is then mapped to a unit circle by a modified Joukowski transformation. A global grid for a two-element airfoil, referred to as Williams' airfoil, is generated by a sequence of inverse mapping procedures and is shown in Fig. 2. The grid cells are of good quality everywhere except near the region between the trailing edge of the main airfoil and the leading edge of the flap. Excessive mesh-lines clustering, large aspect ratio cells, and mesh distortion exist in the interaction region. A local triangular mesh can be used to improve the quality of the grid system in this region.

The Delaunay triangulation method is applied in four steps to generate triangular elements in the unstructured zone enclosed by the surrounding structured meshes and solid surface boundary. The first step is to triangulate the points along the zonal and solid boundaries in order to obtain an initial triangulation. The boundary points are connected to form a series of edges which are used as an "initial front." Each edge is then connected to a selected boundary point to form a triangle that satisfies two conditions. The first condition is called the Delaunay criteria. A new triangle allows no other point to be inside the circumcircle formed by the three points of that triangle. The other condition is that neither of the two newly formed edges can cross any existing edge. The two new edges that form the triangle are then added to the end of the edge array and the process is repeated until nodes are found for each existing edge.

The second and third steps deal with the placement of interior points and a final triangulation, respectively. It is important to place a sufficiently dense mesh of points in high gradient regions such as corner regions, leading- and trailing-edge regions, etc. A combination of C-mesh points around the leading edge and Cartesian mesh points in other parts of the domain are chosen as the interior points. Based on Bowyer's algorithm, a series of new points are added one by one to the existing triangulation by removing triangles close to the point being inserted and reconnecting the new point to the existing nodes in such a way as to form new triangles which satisfy the Delaunay criteria. This procedure is repeated for all new points introduced in the domain.

The final phase of the unstructured-mesh generation is a grid-smoothing procedure. This is necessary because points from overlapping C-mesh and Cartesian-mesh grids sometimes fall too close to each other, resulting in skewed triangles, such as triangles with large aspect ratio. An iterative Laplacian smoothing scheme is applied to improve the overall quality of the unstructured mesh. In addition, an edge swapping procedure is performed at last to ensure that grid points satisfy the Delaunay criterion.

The resulting composite structured and unstructured grid for this geometry could be seen in Fig. 5 of Sec. VI, where computational examples are presented. A similar procedure is followed to generate composite grids for other geometries that will be discussed in Sec. VI.

III. Finite-Volume Scheme and Time-Stepping

Finite-volume Euler method of Jameson[9] and Mavriplis,[4] using a fourth-order Runge-Kutta time-stepping, are adopted to interactively solve for the flows in different zones. These methods are briefly reviewed here only to point out some modifications that are made in the present work.

The Euler equation for two-dimensional inviscid flow in integral form for a region Ω with a boundary $\partial\Omega$ is given as

$$\frac{\partial}{\partial t}\iint_{\Omega} w\,dx\,dy + \int_{\partial\Omega}(f\,dy - g\,dx) = 0 \tag{1}$$

where x and y are Cartesian coordinates and

$$w = \begin{vmatrix} \rho \\ \rho u \\ \rho v \\ \rho E \end{vmatrix}, \quad f = \begin{vmatrix} \rho u \\ \rho u^2 + p \\ \rho uv \\ \rho uH \end{vmatrix}, \quad g = \begin{vmatrix} \rho v \\ \rho uv \\ \rho v^2 + p \\ \rho vH \end{vmatrix} \tag{2}$$

Here, ρ, u, v, p, E, and H are density, velocity components, pressure, total energy, and total enthalpy, respectively. Equation (1) is discretized over individual control volumes (quadrilaterals or triangles) in a cell-centered approximation, in which the flow variables are stored at the center of each cell. The above discretization procedure with the addition of artificial dissipation terms results in a set of ordinary differential equations

$$S_i\frac{dw_i}{dt} + [Q(w_i) - D(w_i)] = 0 \tag{3}$$

where S_i is the area of the cell, and Q is the spatial approximation of fluxes given by the second part of Eq. (1), and D is an appropriately constructed dissipation operator.

The fourth-order Runge-Kutta scheme is used to advance the solution in time from time level n to time level $n + 1$. With the nonlinear operator P defined as

$$P(w) = (1/S)[Q(w) - D(w)] \tag{4}$$

we have

$$\begin{aligned} w^{(0)} &= w^n \\ w^{(1)} &= w^{(0)} - (\Delta t/2)P[w^{(0)}] \\ w^{(2)} &= w^{(0)} - (\Delta t/2)P[w^{(1)}] \\ w^{(3)} &= w^{(0)} - \Delta t P[w^{(2)}] \\ w^{(4)} &= w^{(0)} - (\Delta t/6)\{P[w^{(0)}] + 2P[w^{(1)}] + 2P[w^{(2)}] + P[w^{(3)}]\} \\ w^{n+1} &= w^{(4)} \end{aligned} \tag{5}$$

In the region with structured grid, implicit residual averaging is used to increase the CFL number for better solution convergence. The calculations presented in this work are obtained with a CFL number of 6. In addition, a variable time step, based on the maximum limit set by the local Courant number, and enthalpy damping, are used to accelerate the convergence of the solution.

In the unstructured flow solver, fourth-order Runge-Kutta time stepping is also used to advance the solution in time, this is similar to the structured flow solver. The support of the time-stepping scheme here is increased by an explicitly residual averaging scheme. If the residuals at cell i are

$$R_i(w) = (1/S_i)[Q(w_i) - D(w_i)]$$

they are replaced by

$$\overline{R}_i = \varepsilon R_i + \frac{1-\varepsilon}{3}\sum_{k=1}^{3} R_{ik}$$

where R_{ik} are residuals at three forming points of the triangular cell. The residuals at nodal points are obtained as the average of residuals at all cells having that point in common. ε is a constant which is chosen as 0.6. With this smoothing scheme, the CFL number for the unstructured flow solver could also be increased to about 6.

It is found that the CFL number in the two zones must be similar to facilitate the convergence of the solution in the entire domain.

IV. Dissipative Terms

The structured flow solver uses a blend of second- and fourth-order dissipation terms to prevent odd and even decoupling of the solution. The artificial dissipation for the unstructured flow solver is similarly constructed as a blend of undivided Laplacian and biharmonic operators.

To obtain the fourth-order dissipation term; in the triangular mesh zone an undivided four-point Laplacian operator is first defined as

$$\nabla^2 w_i = \sum_{k=1}^{3} w_k - 3w_i$$

where w represents the flow variables ρ, ρu, ρv, and ρE. The dissipation flux across a cell face ik, delimiting cells i, and its neighbors k, are then calculated as

$$d_{ik} = \varepsilon_{ik}^{(4)} A_k(\nabla^2 w_i - \nabla^2 w_k) \tag{6}$$

where

$$A_k = |u_k\Delta y_k - v_k\Delta x_k| + c_k\sqrt{\Delta x_k^2 + \Delta y_k^2}$$

Here, Δx_k and Δy_k are coordinate increments of the edge, and u_k, v_k, c_k are velocity components and the speed of sound along the edge, respectively, and are taken as the average of the values at cells i and k. The A_k term, which is proportional to the size of the cell face k, and represents the maximum eigenvalue of the Euler equation in the direction normal to

the face, scales appropriately with the time derivative in Eq. (3). In order to more accurately scale the cells which have higher aspect ratios, in the present formulation A_k is not integrated around the boundary of the control volume as it is normally done.

The second-order dissipation term is similarly constructed by replacing $\nabla^2 w_i$ and $\nabla^2 w_k$ in Eq. (6) with w_i and w_k, respectively, so that we have

$$d_{ik} = \varepsilon_{ik}^{(2)} A_k (w_i - w_k)$$

The final form of the dissipative flux is then

$$d_{ik} = \varepsilon_{ik}^{(2)} A_k (w_i - w_k) + \varepsilon_{ik}^{(4)} A_k (\nabla^2 w_i - \nabla^2 w_k)$$

The treatment of the boundary conditions is known to affect the convergence and accuracy of the solution. The wall pressure can be extrapolated from the pressure at the center of the boundary cell using the method given in Ref. 9. However, it is found, in both the structured and unstructured solvers, that the normal pressure gradient $\partial p/\partial n$ is negligible, and the pressure on the boundary surface could be assumed equal to the pressure at the center of the boundary cell.

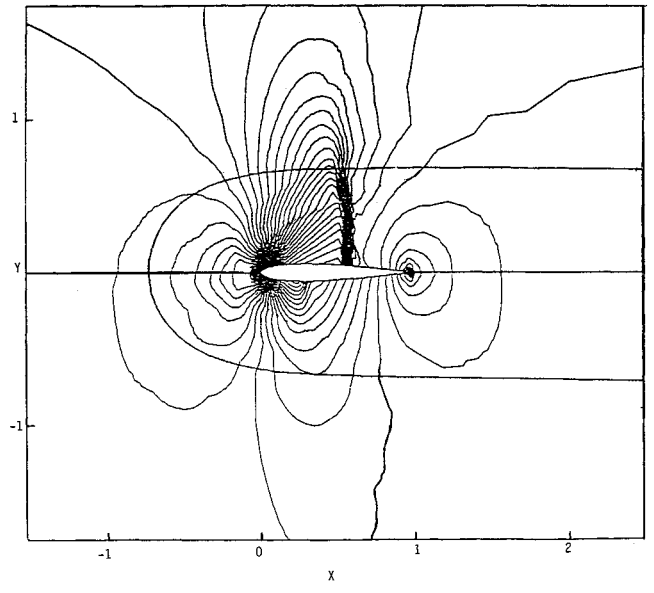

Fig. 3 Isobar solution for NACA 0012 airfoil, using composite grid of Fig. 1. Zonal boundary is shown. $M = 0.8$, $\alpha = 1.25$.

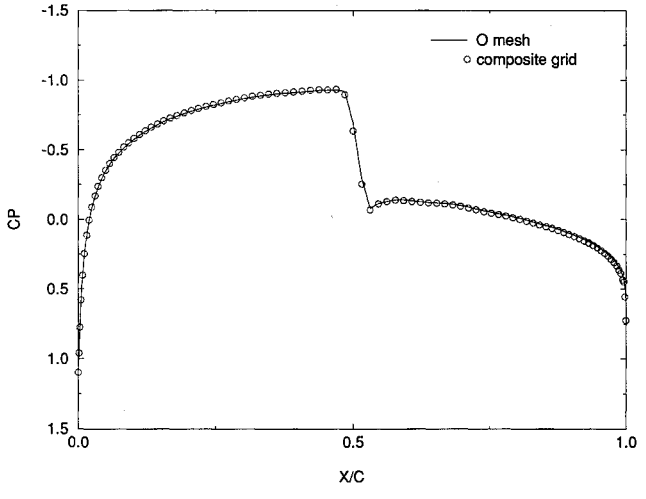

Fig. 4 Comparison of shock location and strength solutions obtained by composite grid and structured O mesh. $M = 0.8$, $\alpha = 0$.

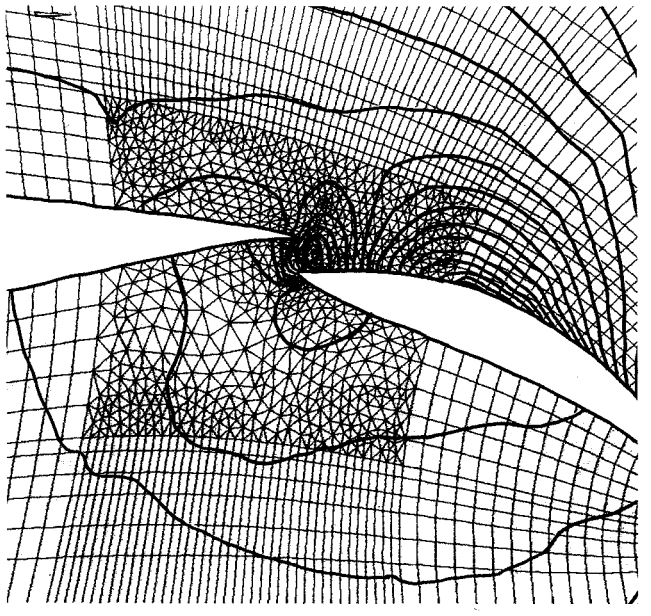

Fig. 5 Isobar contour plots of flow over a two-element airfoil obtained by composite grid. $M = 0.2$, $\alpha = 0$.

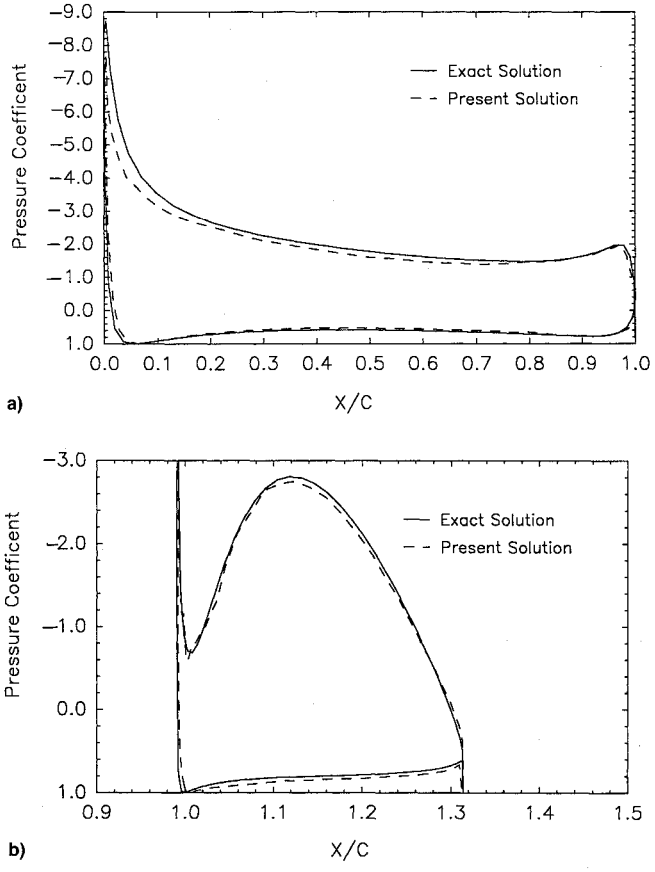

Fig. 6 Comparison of the calculated pressure coefficients at $M = 0.2$, $\alpha = 0$ with the exact incompressible solution, for the two-element Williams' airfoil: a) main airfoil and b) flap.

A more important point, when imposing the solid boundary condition in the unstructured flow solver, however, is that setting the normal components of the fluxes to zero, and only accounting for the pressure terms in the momentum equation, does not necessarily satisfy the flow tangency condition on the boundary. A stronger formulation is needed to ensure this requirement. In the present cell-centered scheme, a stronger form of the boundary condition is imposed in order to com-

Table 1 Comparison of computed force coefficient with the exact results

	Main airfoil, C_L	Flap, C_L	Total, C_L
Present results	2.8304	0.8132	3.6836
Exact solution	2.9065	0.8302	3.7367

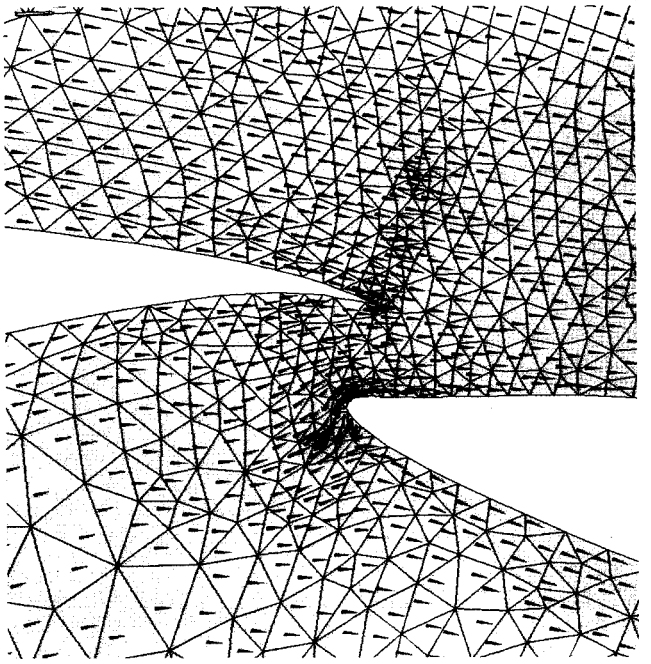

Fig. 7 Direction of the velocity in the unstructured zone, $M = 0.2$, $\alpha = 0$.

pute the artificial dissipation terms more exactly. Flow variables ρ, ρu, ρv, ρE in imaginary cells inside the solid surface are extrapolated based on the assumptions of no normal flux, and equal tangential fluxes between two cells outside and inside the boundary. These values are then used in the calculation of dissipation terms associated with the edges that are on the boundary. This can be shown to be equivalent to explicitly setting velocities to be tangent to the wall, as suggested in Ref. 4.

V. Zonal Interaction Scheme

Communication between neighboring structured and triangular zones could be greatly simplified by choosing point-match boundaries, such that there are common edges between two zones. Mass, momentum, and energy fluxes through the zonal boundaries are conserved by using the values from neighboring zones when calculating fluxes. This requires maintaining information on the grid interaction such as indexes of structured grids next to the boundary triangular meshes, and vice versa.

Careful attention must be given to calculation of dissipation terms for the boundary cells in order to ensure conservation of dissipation terms throughout the flow. Dissipation terms for the triangular, boundary cells are calculated by extracting information from both the structured and unstructured zones and vice versa. Inappropriate treatment of dissipation terms can introduce solution inaccuracy along the zonal boundaries or can produce considerable decoupling of the solution in boundary regions of both zones and contaminate the solution in the entire region. It is also found that comparable CFL numbers and degrees of smoothing in different zones are es-

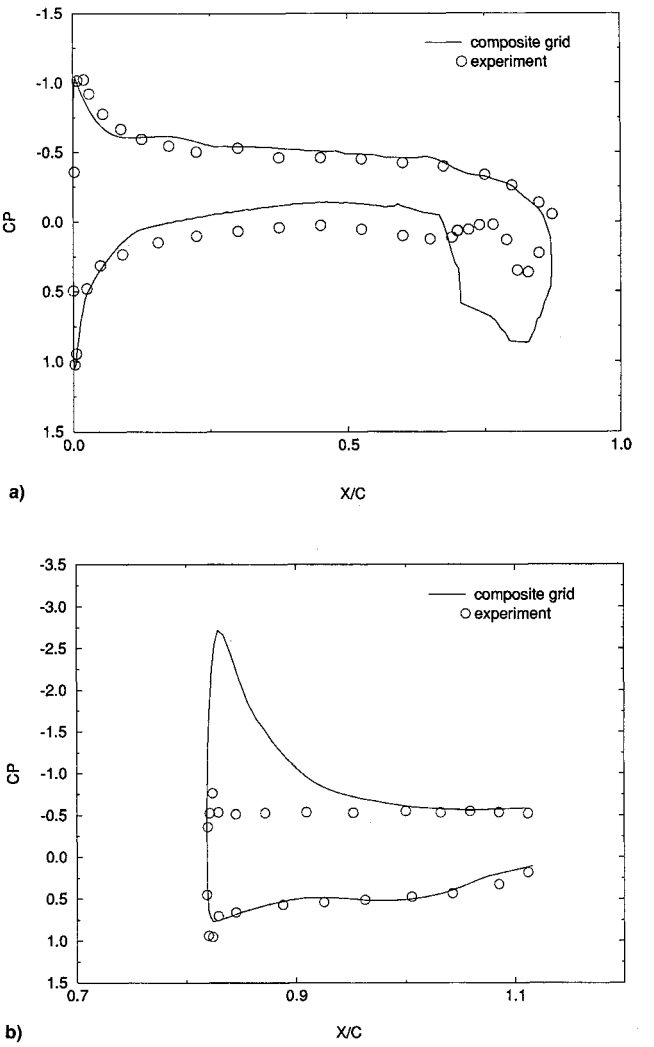

Fig. 8 Comparison of calculated pressure coefficient with experimental results for a two-element airfoil with flap well, $M = 0.105$, $\alpha = 0$: a) main airfoil and b) flap.

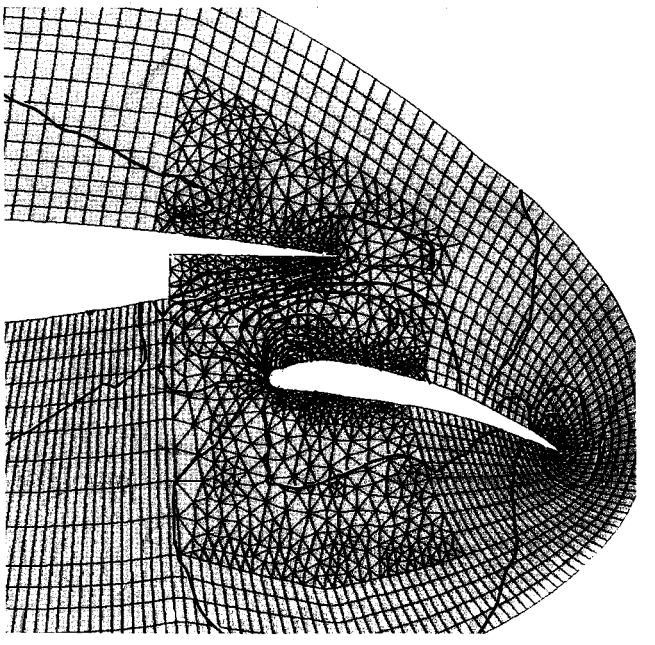

Fig. 9 Isobar contour plots for the two-element airfoil with flap well, $M = 0.105$, $\alpha = 0$.

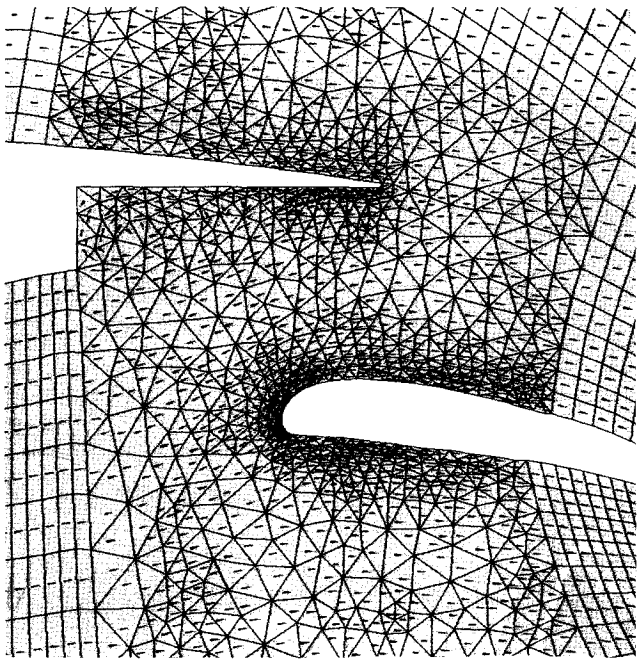

Fig. 10 Direction of velocity in the flap-well region, $M = 0.105$, $\alpha = 0$.

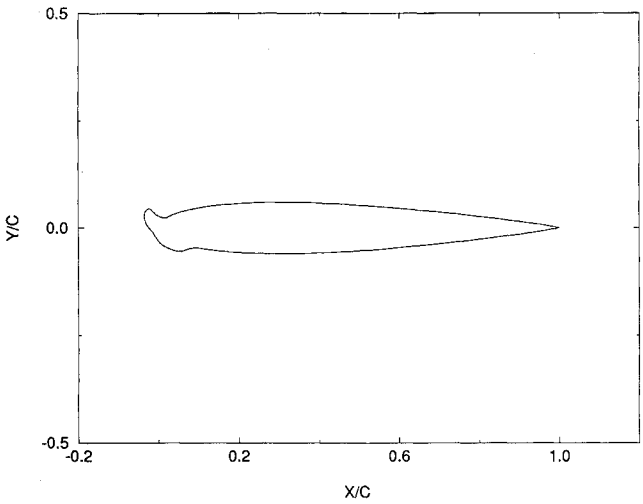

Fig. 11 Eight-minute ice surface on a NACA 0012 airfoil.

sential to improve the overall convergence of the solution in the entire region.

VI. Computational Examples

A prototype problem for two zones with structured C-grid in the near field, around the airfoil and structured H-grid in the far field, is first solved to test the two-dimensional zonal code. A hybrid H/C mesh is generated by conformal mapping procedures. In general, a C-mesh clusters naturally near the leading edge of the airfoil and is more desirable to resolve the higher pressure gradient in this region, whereas the H-mesh is adequate in the far field because of its simplicity and easy application. The C- and H-mesh lines of the hybrid mesh are discontinuous, allowing a more independent grid generation in each zone. This measure could be very useful in more complicated geometries where different components may have different grid-generation requirements. One or several layers of triangular meshes can be generated to serve as a link between structured C- and H-meshes. This example uses one layer of unstructured mesh for this purpose.

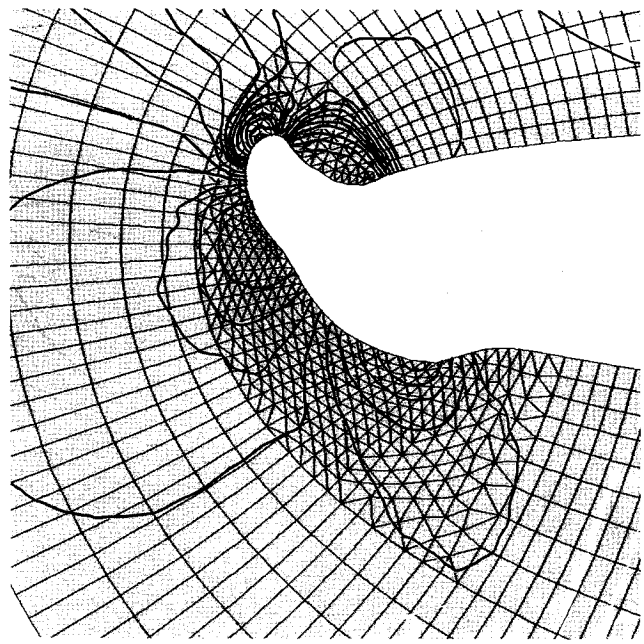

Fig. 12 Isobar solutions for the iced airfoil of Fig. 11. $M = 0.2$, $\alpha = 4$.

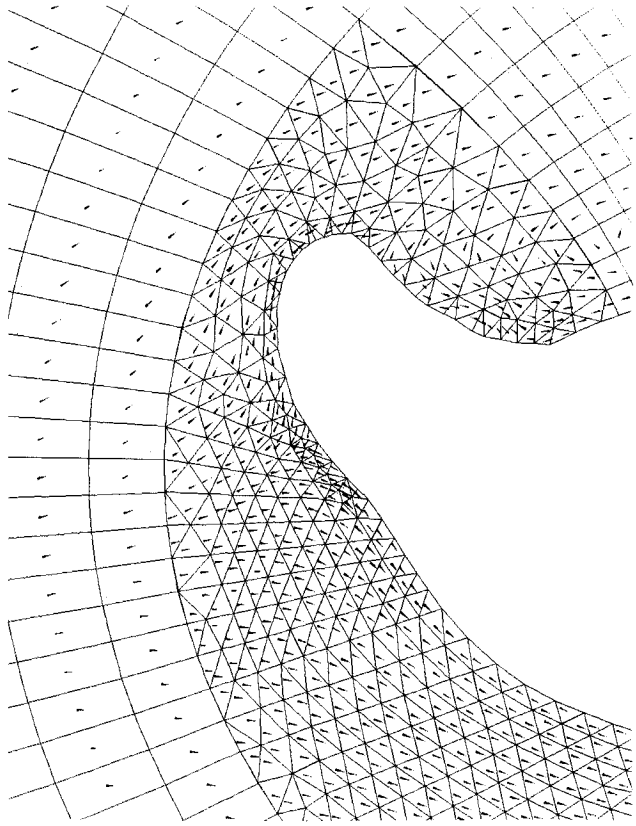

Fig. 13 Direction of velocity vectors in the leading edge of an iced airfoil, $M = 0.2$, $\alpha = 4$.

The isobar solution for NACA 0012 airfoil at Mach number 0.8 is shown in Fig. 3. Conservation of fluxes across zonal boundaries ensures a continuous solution across them. Figure 4, which compares the solution obtained by a composite grid with the solution obtained by using O-mesh only, shows that the location and strength of the shock is predicted very accurately. A CFL number of 6, along with a variable time step, based on maximum limit set by local Courant number, is used

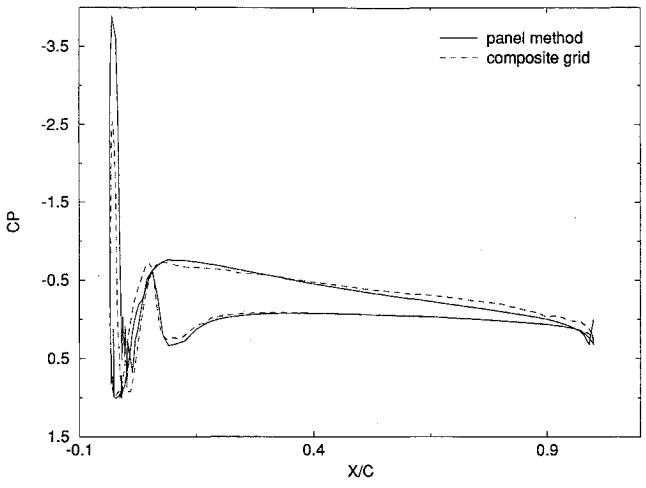

Fig. 14 Comparison of the computed pressure coefficient with surface panel results, $M = 0.2$, $\alpha = 4$.

in both zones. This results in a convergence rate identical to that of the solution obtained with using structure C-mesh alone.

A more complicated example is the two-element Williams' airfoil. An isobar contour plot at Mach number 0.2 is shown in Fig. 5, which indicates a smooth solution across the zonal boundaries. The calculated surface pressure for both the main airfoil and the flap are compared with the exact incompressible solution of Ref. 10 in Fig. 6. The results show good agreement between the two solutions. The compressibility effects at Mach number of 0.2 are less than 2%, according to the Prandtl Glauert rule.

Computed lift coefficients are compared with the exact values in Table 1 and also show good agreement.

Figure 7 shows the direction (not the magnitude) of the velocity in the unstructured zone and indicates that the strong form of the boundary condition discussed earlier in Sec. IV, adequately satisfies the flow tangency requirement on the solid boundary.

A similar solution using multiblock, structured mesh is presented in Ref. 11, where the grid consists of 10,688 cells in 23 blocks. In addition to avoiding a complicated domain decomposition algorithm, the current solution only utilizes 192 $\times$ 32 O-meshes; part of which are replaced by 736 triangles. A purely unstructured solution for a similar multielement airfoil is also presented in Ref. 4. While the total of 5876 nodes used in that calculation is similar to the number of points in the present solution, the data sets required by unstructured algorithm need substantial (approximately 6 times) more storage compared to the present approach.

Similar calculations are performed for a two-element airfoil with a flap well. The configuration chosen has a gap-to-chord ratio of 1% and an overhang of 3%. Calculated pressure coefficients are compared with experimental results[12] in Fig. 8. The experimental data were taken at Mach number 0.105 and Reynolds number (based on chord not extended) of 5.0×10^6. The calculated inviscid solution obviously fails to predict the separation on the upper surface of the flap. The comparison is also very poor in the flap well where the flow is dominated by viscous effects. Isobar contour plots are shown in Fig. 9 and indicate smooth zonal interaction. Minor pressure oscillation in the zonal boundary region near the sharp corner of the flap well could be due to a fairly coarse mesh in this area. Figure 10 shows direction of the velocity vector (not the magnitude) in the unstructured region. Although the equations are inviscid, the addition of dissipation terms have produced viscous flow-like vorticity in the flap-well region. Once again the flow tangency condition is well satisfied by imposing a stronger form of boundary condition.

Our last computational example deals with iced airfoils. The analysis of the aerodynamic performance of iced airfoils has been of great interest to aircraft designers. In order to find ways to prevent ice formation on wings, one needs to accurately predict the flowfield about iced airfoils with various forms of ice shapes.[13] Ice accretion on an airfoil produces very irregular and rough surfaces on the leading-edge region. These shapes normally have concavities and convexities which cannot be modeled using a single zone structured grid. Furthermore, since the ice shape changes continuously, flow calculations require continuous regridding of the computational domain. A composite approach enables the regridding of only a small region near the changing ice shape.

An iced NACA 0012 airfoil with an 8-min ice surface computed using the fortified Lewice program of Ref. 14 is shown in Fig. 11. A composite structured and unstructured grid is generated consisting of 192 $\times$ 32 O-meshes, part of which are replaced by 932 triangular meshes. The unstructured mesh region is extended far enough to cover the irregular ice shape on the leading edge. A converged solution obtained using this mesh is presented in subsequent figures.

Figure 12 shows the isobar solution obtained at $M = 0.2$ and $\alpha = 4$ deg. The contour lines vary smoothly across the zonal boundary indicating that the conservation of fluxes is well satisfied.

Figure 13 shows the velocity vectors in the leading-edge region. This figure clearly indicates that there are multiple stagnation regions where streamlines approach the surface from the far field and are divided in two opposite directions on the surface. There is also a small region of reverse flow on the upper surface. Similar to the previous example, although the equations are inviscid, the addition of dissipation terms produces viscous flow like vorticity behind the ice shape on the upper surface.

The computed pressure distribution on the surface is compared with the surface panel method results in Fig. 14; good agreement is indicated.

VII. Conclusions

The objective of the present work is to develop an efficient and reliable two-dimensional zonal approach, capable of coupling structured and unstructured grid zones. This approach requires considerably less memory compared to using an entirely unstructured mesh capable of handling complex geometries, and takes advantage of the different desirable features of structured and unstructured meshes. An unstructured grid could be used to link different kinds of structured grids which may be necessary due to the requirements of the grid generation method of different components, or reduce regridding effort in problems requiring dynamic mesh. Other potential applications of the composite approach are also discussed.

Computed examples show that accurate and efficient solutions can be obtained by paying careful attention to the grid quality and flux conservation through the zonal boundaries.

References

[1]Watson, D. F., "Computing the *n*-Dimensional Delaunay Tesselation with Application to Voronoi Polytropes," *The Computer Journal*, Vol. 24, No. 2, 1981, pp. 167–172.

[2]Batina, J. T., "Unsteady Euler Algorithm with Unstructured Dynamic Mesh for Complex-Aircraft Aerodynamic Analysis," *AIAA Journal*, Vol. 29, No. 3, 1991, pp. 327–333.

[3]Roe, P. R., "Error Estimates for Cell-Vertex Solution for the Compressible Euler Equations," Inst. for Computer Applications in Science and Engineering Rept. 87-6, NASA CR-178235, Jan. 1987.

[4]Mavriplis, D. J., "Accurate Multigrid Solution of the Euler Equations on Unstructured and Adaptive Meshes," *AIAA Journal*, Vol. 28, No. 2, 1990, pp. 213–221.

[5]Venkatakrishnan, V., and Mavriplis, D. J., "Implicit Solvers for Unstructured Meshes," AIAA Paper 91-1537, June 1991.

[6]Venkatakrishnan, V., and Batina, J. T., "Application of Direct Solvers to Unstructured Meshes for the Euler and Navier-Stokes

Equations Using Upwind Schemes," AIAA Paper 89-0364, Jan. 1989.

[7]Sanjay, R., Madavan, N. K., and Rajagopalan, R. G., "A Hybrid Structured-Unstructured Grid Method for Unsteady Turbomachinery Flow Computations," AIAA Paper 93-0387, Jan. 1993.

[8]Halsey, N. D., "Calculation of Compressible Potential Flow About Multielement Airfoils Using a Source Field Panel Approach," AIAA Paper 85-0038, Jan. 1985.

[9]Jameson, A., Schmidt, W., and Turkel, E., "Numerical Solution of the Euler Equation by Finite-Volume Method Using a Runge-Kutta Time-Stepping Scheme," AIAA Paper 81-1259, June 1981.

[10]Williams, B. R., "A Comparison of the Surface-Source Solution with an Exact Solution for the 2-D Inviscid Flow About a Slotted-Flap Airfoil," Royal Aircraft Establishment Technical Rept. 72008, March 1972.

[11]Stewart, M., "A General Decomposition Algorithm Applied to Multi-Element Airfoil Grids," AIAA 90-1606, Jan. 1990.

[12]Cebeci, T., private communication, Long Beach, CA.

[13]Shaw, R. J., Potapczuk, M. G., and Bidwell, C. S., "Prediction of Airfoil Aerodynamic Performance Degradation Due to Icing," *Numerical and Physical Aspects of Aerodynamic Flows, IV*, edited by T. Cebeci, Springer-Verlag, New York, 1990.

[14]Cebeci, T., Chen, H., and Alemdaroglu, N., "Fortified Lewice with Viscous Effects," *Journal of Aircraft*, Vol. 28, No. 9, 1991, pp. 564–571.